J Mater Sci (2009) 44:4930–4938
DOI 10.1007/s10853-009-3752-9

Quasi-static cyclic loadings induced inelastic deformation in a Zr-based bulk metallic glass under nanoindentation

A. Tekaya · S. Labdi · T. Benameur · A. Jellad

Received: 2 June 2009 / Accepted: 15 July 2009 / Published online: 29 July 2009

Abstract Cyclic nanoindentation tests were carried out on $Zr_{50}Cu_{40}Al_{10}$ bulk metallic glass (BMG). From the designed quasi-static and incremental cyclic experiments at loading rates ranging from 250 to 2500 μN/s and at ambient temperature, we observed significant difference in inelastic deformation as a function of solicitation modes. Under incremental cyclic loadings, the hardness of the BMG increased each time when the sample was reloaded immediately after unloading and then gradually reduced before the next unloading. In contrast, we found that quasi-static cyclic loadings induced a mechanical softening which appears to be dependent on the number of cycles and the loading rates. The inelastic deformation was studied by analysing the remnant indent morphology using atomic force microscopy. A free-volume mechanism was proposed for interpreting these observations quantitatively.

Introduction

Bulk metallic glasses (BMGs) remain as interesting class of materials for both basic and applied research as they posses a number of remarkable functional and structural properties. While some properties, for example, thermal conductivity, expansion and specific heat, are not unusual, the corrosion resistance and low temperature dependence of resistivity are potentially attractive [1–4]. Despite the extremely high strength, large elastic strain limit combined with relatively high fracture toughness, as well as good wear resistance of BMGs, they suffer a strong tendency for shear localization and fail catastrophically on one dominant shear band in tensile tests at ambient temperature [5, 6]. In constrained geometries such as in bending or uniaxial compression, they are capable of legitimate plasticity due to generation of multiple shear bands [7]. However, the current works have been polarized towards finding, optimizing new glass-forming compositions [8] and developing fundamental understanding of plastic deformation and fracture mechanisms in monolithic BMGs. Indeed, El-Hadek and Kassem [9] reported an improvement of fracture strength and strain of Cu-based BMG with the addition of 1 at% Si and Sn. The achievement of homogeneously distributed nano-sized precipitates (2–5 nm in diameter) induces a modification from single to multiple shear plane fracture mode.

So far, recent efforts have been made to elucidate their shear band evolution patterns after monotonic loading experiments [10, 11]. Moreover, nanoindentation has been widely used to detect individual shear band events in metallic glasses, with high accuracy [12, 13]. It was observed that the shear band size and density varied with the applied strain rate. Indeed, the excellent time and displacement resolution of a nanoindenter, for instance, has been demonstrated in the analyses of the pop-in size and distribution under various loads and strain rates [14, 15]. In conventional nanoindentation, loading causes both elastic and plastic deformation under the indenter, while unloading is dominated by recovery of the elastic deformation. A variation to this test is cyclic indentation where the sample is reloaded immediately to even higher loads/depths than the previous loading cycle. The unloading–reloading paths do not necessarily overlap in crystalline alloys and

A. Tekaya · T. Benameur (✉) · A. Jellad
LGM-LAB-MA05, ENIM, Université de Monastir,
5019 Monastir, Tunisia
e-mail: t.benameur@enim.rnu.tn

S. Labdi
LMN-LAB-EA2540, Université d'Evry Val d'Essonne,
91000 Evry, France
e-mail: sid.labdi@univ-evry.fr

resulting in hysteresis loops (strain hardening) or disparities (strain softening) due to sensitive dislocation–microstructure interactions detectable in the unloading–reloading curves [16].

Although metallic glasses do not exhibit strain hardening due to the absence of dislocation-mediated plasticity, both hardening and recovery in a Zr-based BMG under controlled nanoindentation conditions have been reported [13]. Furthermore, introduction of a compressive residual stress through shot peening has also been observed [17]. A question that is yet to be answered is: what are the origins of kinematic irreversibility in monolithic BMGs?

In this study, it is thought that using cyclic nanoindentation tests in quasi-static and incremental solicitation modes could be very effective to extract sensitive information about BMG behaviour such as possible shifts in nanoindentation curves or in the yield point that may arise due to local structural changes. While quasi-static cyclic loading at a maximum applied force $F_{Max} = 3750$ μN induced inelastic deformation in $Zr_{50}Cu_{40}Al_{10}$ amorphous alloy, incremental cyclic loading shows a little increase of hardness upon each reloading. The continuous increase of inelastic deformation under cyclic solicitation at constant F_{Max} has never been observed. The identification of changes in the dissipated energy during deformation, the indented morphology by the variation of loading rate using atomic force microscope and image processing of the observed surface topography is developed.

Experimental procedures

The material used in this study is $Zr_{50}Cu_{40}Al_{10}$ (at.%) BMG prepared by arc-melting a mixture of pure elements with purities ranging from 99.9 to 99.99% and under a purified argon atmosphere. The amorphicity was examined using a monochromatic X-ray diffractometer. Instrumented nanoindentation experiments were conducted using a Triboindenter (Hysitron). This system is connected to a digital instrument D3100 AFM. The load and depth resolutions are 1 nN and 0.04 nm, respectively. A pyramidal diamond Berkovich tip with a total included angle of 142.3° and a finite tip radius of 100 nm has been used. Prior to nanoindentation test, the specimens were mechanically polished to a mirror finishing and tested at constant loading rates. Fused silica was used as a standard sample for the initial tip calibration and to determine the area $A(h)$ function. Monotonic and quasi-static cyclic loading were conducted at different loading rates ranging from 250 to 2500 μN/s at a maximum load of 3750 μN as well as incremental cyclic loading experiments with a load varying from 1000 to 6000 μN. At least 10 tests were repeated at each condition and the results presented are reproducible within the standard deviation of less than 5%. A dwell period of 120 s was imposed to correct for the thermal drift. Selected indents were imaged using the indenter tip itself.

Results and discussion

When multiple unloading–reloading tests were conducted during nanoindentation experiments using different loading modes at various loading rates, a peculiar softening behaviour was observed. Figure 1 shows the load versus time functions used in the nanoindentation processes using Hysitron Triboscope. The indentation functions consisted of a conventional monotonic loading (Fig. 1a), quasi-static cyclic loadings (Fig. 1b) and incremental cyclic loadings (Fig. 1c) at different loading rates ranging from 250 to 2500 μN/s with a maximum applied load of 6000 μN. From the load–displacement curves, the hardness H and reduced Young's modulus E_r values were evaluated using the model of Oliver and Pharr [18].

Shown in Fig. 2 are nanoindentation load–displacement curves for an applied load of 3750 μN at different loading rates of 250, 500 and 2500 μN/s and illustrate the presence of a discrete displacement bursts, corresponding to a sudden penetration of the indenter in the material without increase of the applied strength. This phenomenon named "pop-in" or serrations (shown in the inset) have been already reported in literature and it has been generally believed that are associated with a plastic flow consequence of the activation of individual shear bands underneath the indenter tip [19].

As expected, with increasing the loading rate, the pop-in events are less clear in load–displacement curves as

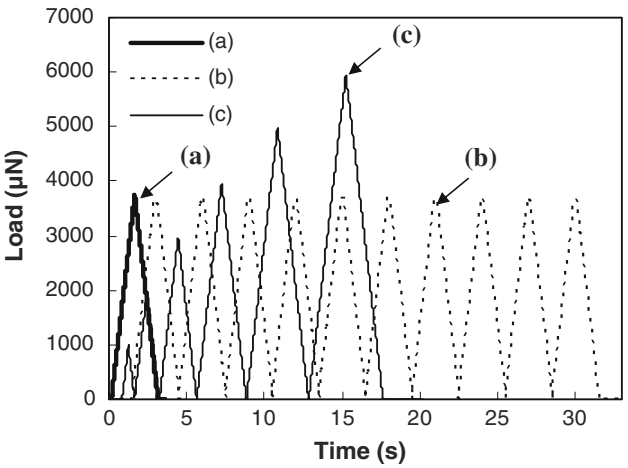

Fig. 1 Load versus time functions used in the nanoindentation processes using Hysitron nanoindenter: (*a*) Monotonical loading. (*b*) Quasi-static cyclic loading. (*c*) Incremental cyclic loading

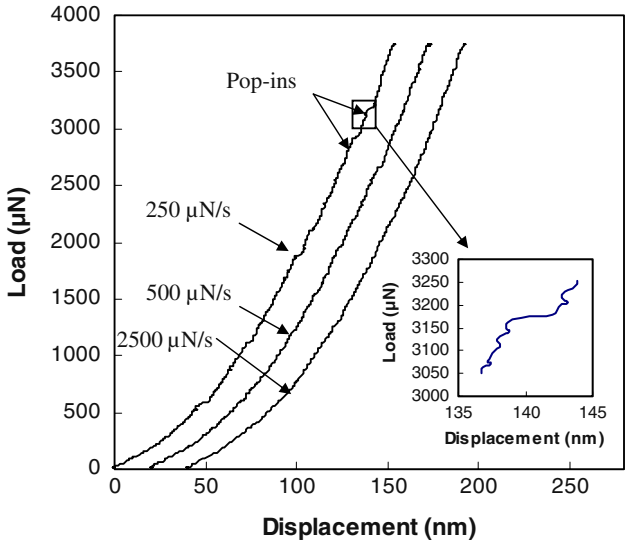

Fig. 2 Load–displacement curves obtained for $Zr_{50}Cu_{40}Al_{10}$ BMGs at a loading of 3750 μN and at different loading rates. Curves are offset from the origin for clear viewing. The *inset* shows the pop-ins phenomena

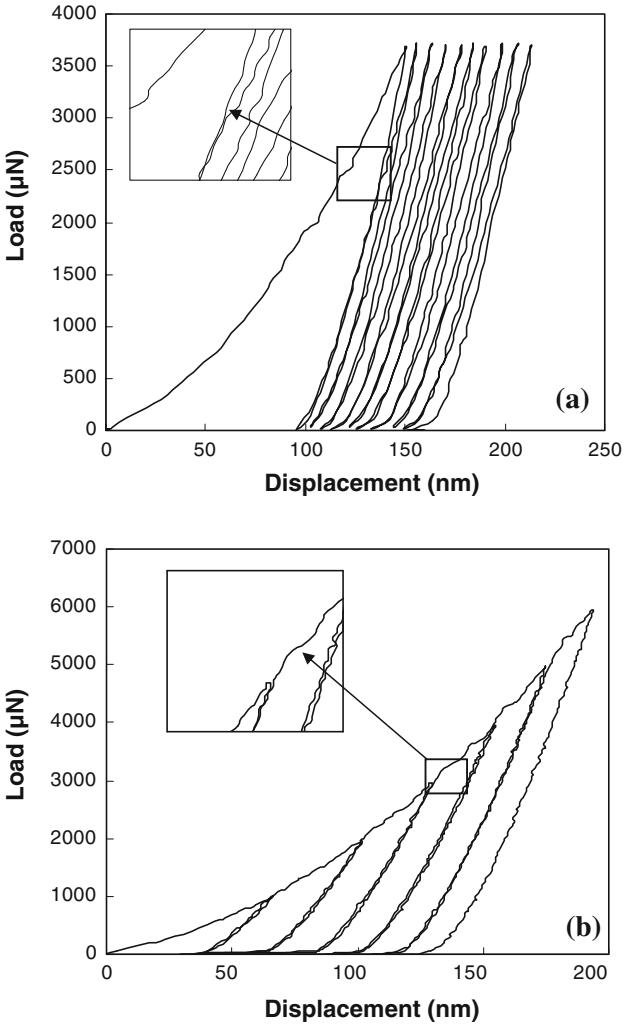

Fig. 3 Load–displacement plots of $Zr_{50}Cu_{40}Al_{10}$ at: **a** Quasi-static cyclic loading. **b** Incremental cyclic loading with loading rate of 500 μN/s

revealed in Fig. 2; this phenomenon was attributed to the lack of resolution of the experimental setup [20]. However, Schuh and Nieh suggested that the absence of pop-in events at high loading rates was rather caused by the kinetic limitation on the nucleation of shear bands [19]. Indeed, it is possible that the nucleation and propagation of a single shear band is sufficient to accommodate the applied strain, if the strain rate applied is low, resulting in discrete pop-in events, whereas the high applied strain rate will require the simultaneous activation of multiple shear bands and this suppresses the pop-in event, leaving with a smooth load–displacement curve. It is recognized that shear localization or shear band formation in BMGs is a direct consequence of strain softening caused by the local production of free volume as long as the relaxation does not completely induce modification of structural order after the shear process, as observed in our previous work [21, 22]. We take a step further on the observation of continued local inelastic deformation under cyclic nanoindentation at constant maximum load F_{Max} and for a wide range of loading rates.

A typical load–displacement plot of $Zr_{50}Cu_{40}Al_{10}$ for both quasi-static and incremental cyclic loadings at the same loading rate of 500 μN/s are shown in Fig. 3a, b, respectively. In the case of quasi-static cyclic loadings, the path of reloading curves does not follow completely the unloading curve of previous cycles. When sections of the curve containing the unloading–reloading paths are magnified, it becomes clear that they do not overlap but form an open jaw as seen in the inset of Fig. 3a. The open jaw signifies that the sample behaviour was softer on reloading compared to the previous unloading path. Note that the disparity between the unloading and reloading paths increases as the indentation depth of cycling increases. However, in incremental cyclic loadings mode, it is observed that the onset of yielding upon each reloading is always noted to take place at a higher load in the order of 7% higher than the maximum load reached in the previous cycle (inset of Fig. 3b). Also noted in the figure is that, in the reloading path, the deformation continues to be elastic.

In trying to quantify the increase of hardness in each cycle in the incremental cyclic loadings mode, the work of indentation approach can be used to determine accurate hardness values [23]; however, as first approximation, the hardness is taken proportional to the stress and equals to P/A, where P is the applied load and A is the indentation area calculated by the area function of an ideal Berkovich indenter tip that is equal to $A = 24.5h^2$ [20]. Figure 4

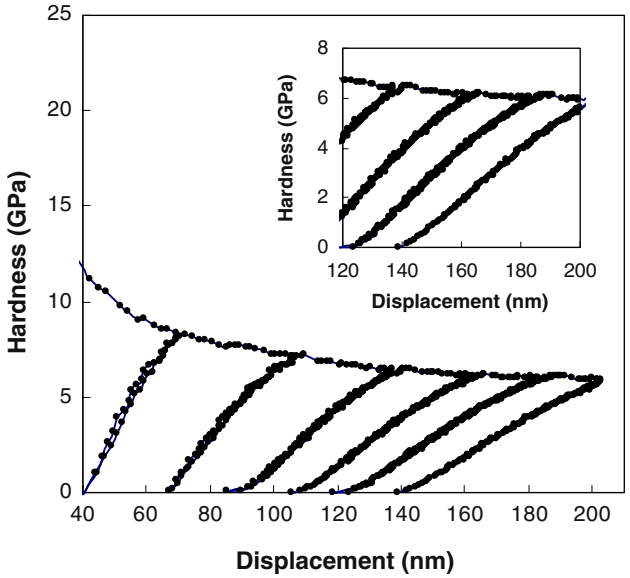

Fig. 4 Hardness versus depth of penetration for incremental cyclic loading at 2500 μN/s

shows the evolution of hardness as a function of penetration depth. A moderate increase of hardness in the range of 2–5% is found upon each reloading (inset of Fig. 4) followed by a gradual diminution and the load–displacement curve returns to where it should be for the next unloading–reloading cycle.

Figure 5a, b reveals the load–displacement curves obtained in the case of quasi-static and incremental cyclic loadings at different loading rates. The effect of variation of the loading rates on the mechanical response of Zr-based metallic glasses under the two loading modes is clearly illustrated. It is worth noting that in quasi-static cyclic mode and mainly after the first cycle, the depth of penetration increases with increasing the number of cycles at $F_{\text{Max}} = 3750$ μN and seems dependent on the loading rates as seen in Fig. 5a. Indeed, at higher loading rate in the order of 2500 μN/s, the reloading–unloading cycles overlap showing an important elastic recovery. However, in Fig. 5b, the curves obtained in the case of incremental cyclic loading at 500, 1000 and 2500 μN/s loading rates essentially overlap with one another, indicating that the moderate increase and reduction of hardness, a so-called "hardening and recovery" mechanisms, are independent of loading rate at room temperature [13]. They suggested that during unloading process, with a sudden reduction of the applied shear stress, the driving force for free volume accumulation decreases, and the free volume annihilation process takes over, as described in Steif et al.'s flow equation for metallic glasses [2]. This results in a relaxation of free volume, which causes the immediate arrest of propagating shear bands. Upon the next reloading, all

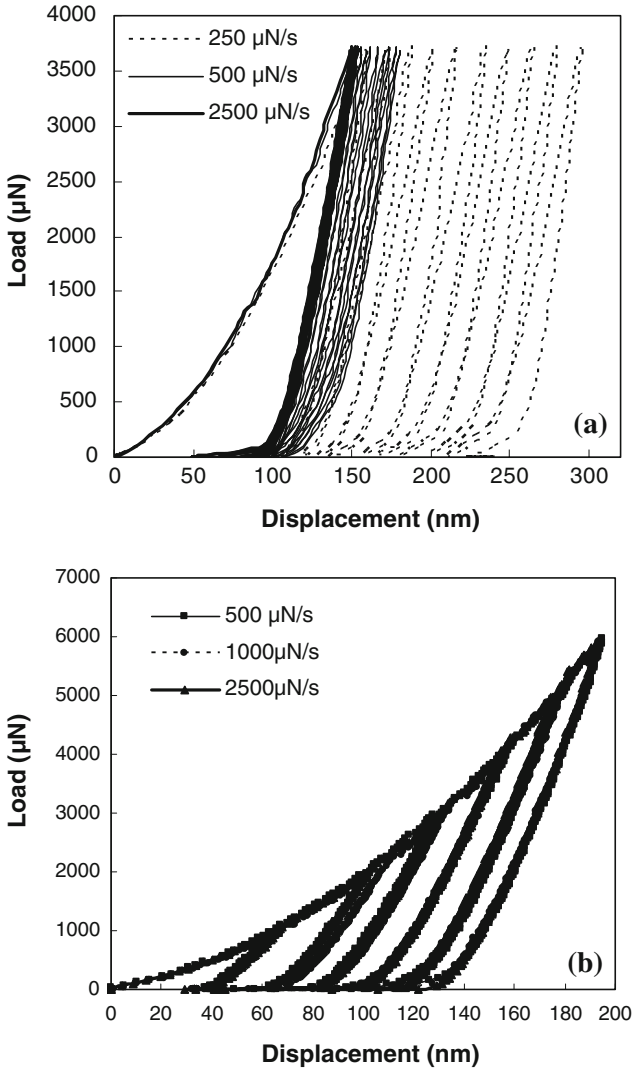

Fig. 5 Load–displacement curves of **a** quasi-static at $F_{\text{Max}} = 3750$ μN and **b** incremental cyclic loading at different loading rates

previous shear bands were already arrested and the free volume accumulation process remains sluggish at room temperature. This results in a moderate increase in hardness (the hardening phenomenon). After the stress is increased to the yielding point, multiple shear bands start to initiate and propagate again. The increased temperature and free volume in the propagating shear bands will then cause the reduction of hardness again (the recovery phenomenon). It is interesting to mention that in incremental cyclic loading, the measured hardness is actually an average value resulted from a mixture of propagating shear bands, arrested shear bands and undeformed regions. In the quasi-static cyclic loading mode, the measured hardness is an average value resulted from a mixture of only propagating and arrested shear bands. This results in an increase of inelastic deformation as a function of number of cycle and strain rate.

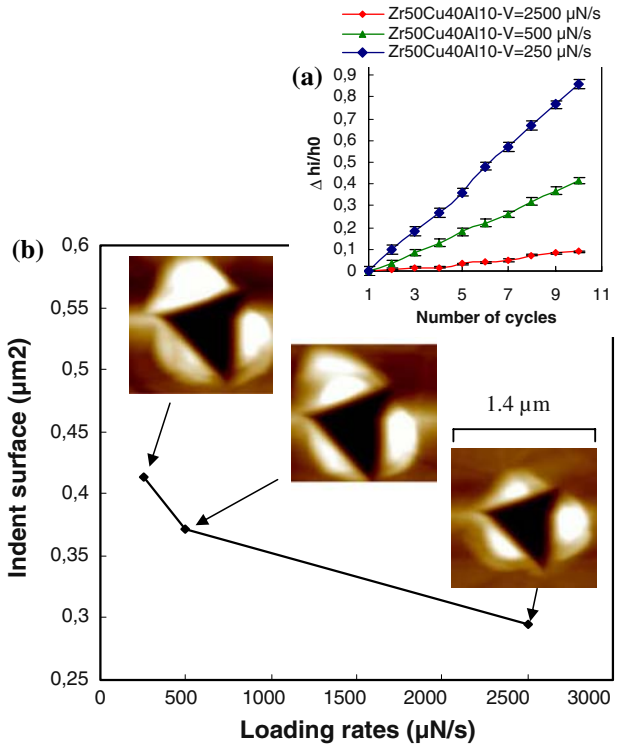

Fig. 6 Evolution of **a** relative depth of penetration $\Delta h_i/h_0$ versus the number of cycles and **b** indent surfaces areas versus the loading rates, for quasi-static cyclic loading at a loading of 3750 µN and at loading rates of 250, 500 and 2500 µN/s

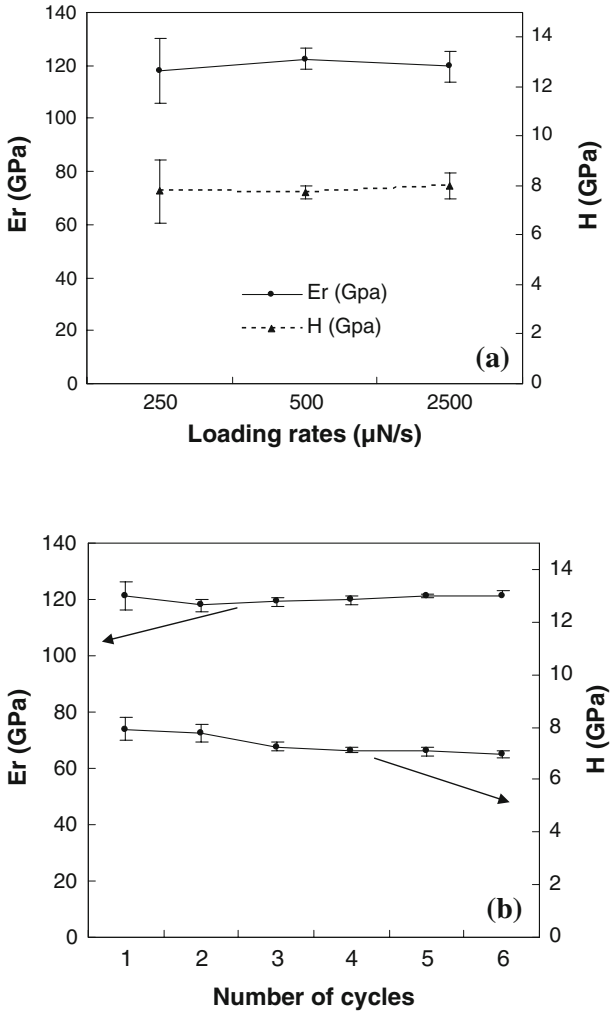

Fig. 7 Plot of indentation hardness and reduced modulus versus **a** loading rate for monotonic loading at a load of 3750 µN and **b** number of cycles for incremental cyclic loading at loading rate of 2500 µN/s

By analysing the enhanced inelastic deformation during the cyclic nanoindentation at constant peak load $F_{\mathrm{Max}} =$ 3750 µN through the evolution of the relative depth of penetration defined by $\Delta h_i/h_0$ ratio, where h_0 is the maximum penetration depth reached in the first cycle and $\Delta h_i = h_i - h_0$, where h_i is the maximum penetration depth reached at the cycle number i. Figure 6a shows plots of $\Delta h_i/h_0$ ratio as a function of loading rates and the number of cycles. The decrease of the relative depth of penetration is estimated to be ~88% when the loading rate is increased from 250 to 2500 µN/s. Further evidence is also deduced from AFM topographic analyses of remnant indent by measuring the imprints surface obtained after ten cycles of loading at $F_{\mathrm{Max}} = 3750$ µN for 250, 500 and 2500 µN/s loading rate as seen in Fig. 6b. The decrease of indents surface by about 28% when the loading rate increased from 250 to 2500 µN/s suggests that elastic recovery increases significantly at higher loading rate.

Moreover, the influence of the number of cycles used in cyclic experiments on the mechanical properties such as hardness and reduced modulus measurements were plotted versus the loading rates, and are shown in Fig. 7a, b. For the monotonic loadings (Fig. 7a), the hardness H increases by 3% from 7.76 ± 1.27 to 7.97 ± 0.53 GPa with increasing the loading rate up to 2500 µN/s. The Young's modulus of the metallic glass E can be obtained from:

$$\frac{1}{E_{\mathrm{r}}} = \frac{1-\upsilon^2}{E} + \frac{1-\upsilon_i^2}{E_i}$$

where E and υ are Young's modulus and Poisson's ratio, respectively of the sample and $E_i = 1141$ GPa and $\upsilon_i = 0.07$ are the corresponding parameters for a Berkovich diamond indenter used in this work. The E/H ratio of $Zr_{50}Cu_{40}Al_{10}$ decreased from 14.76 to 14.57 with the increase of the loading rate. For the incremental cyclic loadings at 2500 µN/s (Fig. 7b), the hardness decreases by ~12% from 7.92 ± 0.44 GPa in the first cycle to 6.95 ± 0.12 GPa in the sixth cycle. While the elastic modulus is found nearly constant, the hardness decreases with increasing the applied load. This phenomenon of softening that causes indentation size effect (ISE) in metallic glasses

has been recently reported [24, 25]. The detailed mechanism of this effect is not well understood; however, the ISE was attributed to a reduction in the shear band density with decreased peak load as well as to the contribution of friction between indenter facets and the test specimen [26].

Furthermore, from the integral of the load–displacement curves, as a function of the number of cycles in the case of quasi-static cyclic loading and incremental cyclic loading, we plotted the W_p/W_t ratio of the dissipated energy during nanoindentation, where W_p is the plastic energy and W_t the total energy ($W_t = W_p + W_e$; W_e is the elastic energy), as shown in Fig. 8a, b. One can see a marked drop of the ratio W_p/W_t after the second cycle, estimated to be nearly 70% at a loading rate of 250 μN/s and ~90% at 2500 μN/s. Moreover, a wavy-like variation of W_p/W_t ratio versus the number of cycles is observed in the quasi-static mode, as

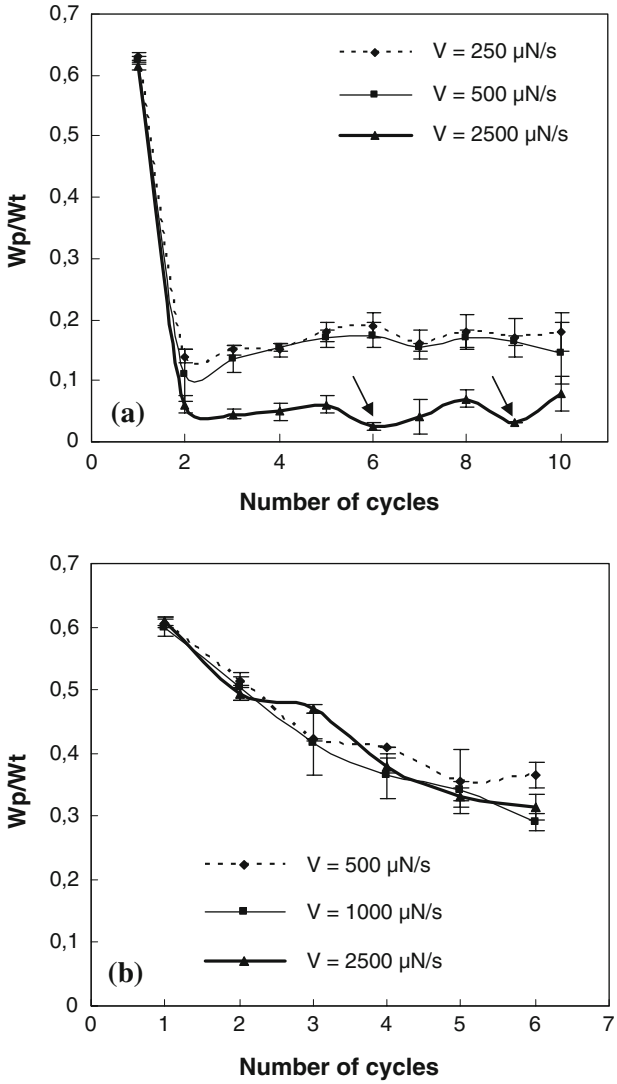

Fig. 8 Evolution of the ratio W_p/W_t with the indentation number of cycles for **a** quasi-static cyclic loading and **b** incremental cyclic loading at different loading rates

indicated by arrows in Fig. 8a. This behaviour illustrates the absence of strain-induced hardening as cyclically loaded at constant $F_{Max} = 3750$ μN allows further inelastic deformation. The results suggest that flow is not only a stress relaxation process but also the dynamic of shear bands propagation that may play a key role in the plasticity of Zr-based BMG. In fact, in cyclic nanoindentation configuration at constant peak load, upon the next reloading of the deformed volume, subtle changes to the glass structure beneath the indenter tip must be occurring to produce the apparent softening trend observed here. The nucleation and propagation of the arrested shear bands are expected and only a few of these shear bands extend onto the indentation surface. This results in competition between nucleation of shear bands, which increases inelastic deformation, and propagation of shear bands to sample surface, which induces a reduction of shear bands density (increasing the elastic recovery; W_e/W_t ratio), as revealed from the evolution of the residual indentation imprint with strain rate shown in Fig. 6b. It is suggested that the variation observed in plastic energy dissipation might be caused by the fact that at least some of the shear bands are terminated when they reach the sample surfaces in a similar way as dislocation propagation and termination in a crystalline material. The comparison with the incremental cyclic solicitations mode for the same glassy alloy indicates that the drop of W_p/W_t ratio is less important and the influence of loading rate is not evident as seen in Fig. 8b. In this cyclic nanoindentation mode, such loading guarantees that virgin material is continually accessed from cycle to another as a consequence of imposed increment of 1000 μN. If the nucleation rate is faster than the applied strain rates, then a weak or no strain rate effect is expected. This is the case of some published data using a very limited strain rate range [27, 28] and observed in the incremental cyclic nanoindentation tests.

An alternative way to access load–displacement data is through the evolution of the elastic recovery parameter h_e/h_{max}, with h_e and h_{max} being the elastic depth and maximum indentation depth, respectively. An obvious advantage of using the h_e/h_{max} ratio is that it can be directly obtained from the unloading curve and is very sensitive to any change in the real contact area caused by the existence of residual stresses. Figure 9a, b shows the variation of h_e/h_{max} ratio as a function of the number of cycles and loading rate for the quasi-static cyclic loading (Fig. 9a) and the incremental cyclic loading (Fig. 9b). It is worth noting that in quasi-static solicitations mode of Zr-based BMG, the h_e/h_{max} ratio shows a peculiar behaviour by analogy to that seen in nanoindentation of crystalline materials, where the effect of compressive residual stress increases the h_e/h_{max} ratio, that is, the elastic recovery of indentation, while the tensile residual stress reduces the h_e/h_{max} ratio

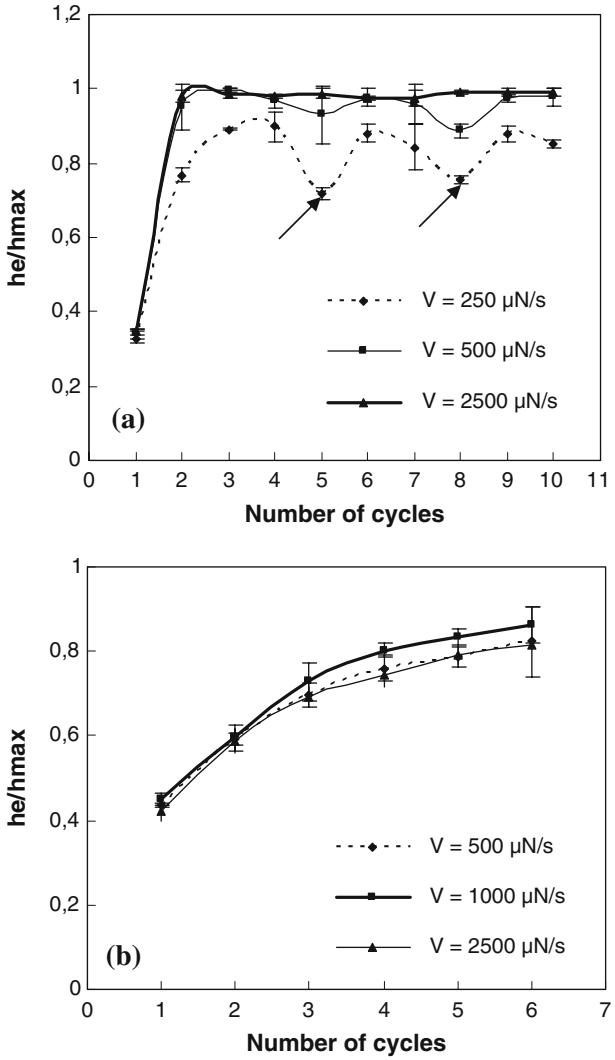

Fig. 9 Evolution of h_e/h_{max} ratio as a function of the number of cycles at different loading rates for **a** quasi-static and **b** incremental cyclic loading

[29]. This is expected in work hardening material; after numerous loading cycles, the unloading process of indentation becomes a pure elastic process and the introduction of compressive stress will tend to push the indenter up more, which results in more elastic recovery, while the introduction of tensile stress will give an opposite effect, which induces less elastic recovery. Interestingly, it is noted that in the Zr-based BMG with no strain hardening due to the lack of dislocation-mediated plasticity, the h_e/h_{max} ratio gradually increases to reach a maximum, apparently suggesting nearly a pure elastic behaviour and then gradually diminishes down to a minimum as a function number of cycles, as shown by arrows in Fig. 9a.

In contrast, under the incremental cyclic solicitations, the h_e/h_{max} ratio increases as to reach a plateau and virtually rate independent as seen in Fig. 9b.

The dependence of hardness H on the number of cycles at different loading rates or strain rates for both cyclic loading modes is plotted in Fig. 10a, b. One can notice, in the case of quasi-static cyclic loading, a significant

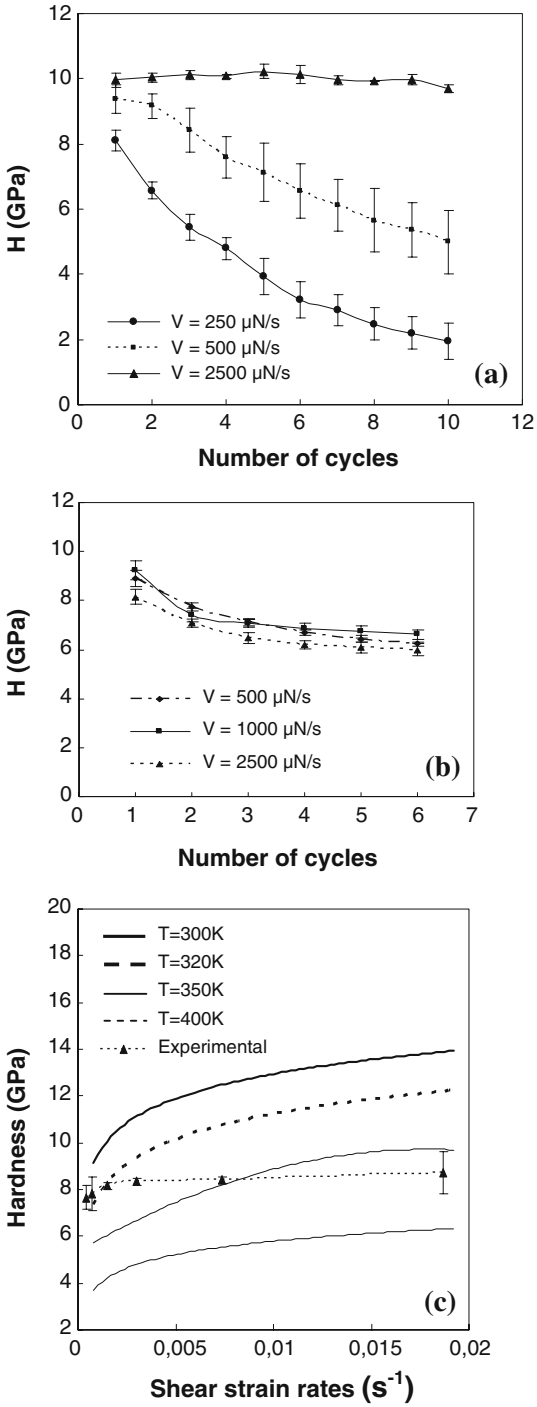

Fig. 10 Hardness as a function of the number of cycles at different loading rates for **a** quasi-static and **b** incremental cyclic loadings. **c** Comparison of experimental hardness versus shear strain rates and numerical values calculated at different temperatures

variation of the hardness. The latter decreases from 6.01 ± 0.15 to 1.74 ± 0.4 GPa at 250 μN/s after ten cycles; however, at higher loading rate 2500 μN/s, the hardness decreases from 6.61 ± 0.13 to 6.46 ± 0.14, as illustrated in Fig. 10a. This phenomenon is not associated to ISE as the load is kept constant; moreover, this is not the case for the incremental cyclic loadings, where the hardness decreases from 8.91 ± 0.31 to 6.24 ± 0.25 GPa and from 8.15 ± 0.34 to 5.48 ± 0.08 GPa at loading rate of 250 and 2500 μN/s, respectively (Fig. 10b).

Following Schuh et al., the hardness can be approximately considered to be proportional to its shear stress τ and $H = 3\tau$ is a good approximation for a variety of amorphous alloys [30].

Based on free volume theory, Steif et al. have derived a flow equation for metallic glasses expressed as [2]

$$\dot{\gamma} = \frac{\dot{\tau}}{\mu} + 2f \exp\left[-\frac{\alpha}{\xi} - \frac{\Delta G^{\mathrm{m}}}{k_{\mathrm{B}}T}\right] \sinh\left(\frac{\tau\Omega}{2k_{\mathrm{B}}T}\right) \quad (1)$$

where $\frac{\partial\gamma}{\partial t}$ is the constant strain rate; $\dot{\tau}$ is the rate of change of applied stress; ξ is the concentration of free volume defined by $\xi = v_{\mathrm{f}}/v^*$, where v_{f} is the average free volume per atom and v^* is a critical volume ($\approx 0.8\ \Omega$); α is a geometrical factor; f is the frequency of atomic vibration; ΔG^{m} is the activation energy; Ω is the atomic volume; k_{B} is the Boltzmann's constant; and T is the absolute temperature. According to Spaepen, the free volume is created by an applied shear stress τ and annihilated by a series of atomic jumps; the net rate of change of the free volume concentration, ξ, is given by [31]

$$\frac{\partial\xi}{\partial t} = f \exp\left[-\frac{\alpha}{\xi} - \frac{\Delta G^{\mathrm{m}}}{k_{\mathrm{B}}T}\right] \left\{\frac{2\alpha k_{\mathrm{B}}T}{S\xi v^*}\left(\cosh\frac{\tau\Omega}{2k_{\mathrm{B}}T} - 1\right) - \frac{1}{n_{\mathrm{D}}}\right\} \quad (2)$$

where n_{D} is the number of atomic jumps required to annihilate v^* and $S = 2/3((1+\upsilon/1-\upsilon)\mu)$, υ is the Poisson's ratio, and μ is the shear modulus.

We have tracked by numerically solving Eqs. 1 and 2 to determine the $\tau_{\max}$ which induces localization with initial conditions $\tau\ (t = 0) = 0$, $\xi = 0.008$ [32], and the physical and mechanical parameters of $Zr_{50}Cu_{40}Al_{10}$ metallic glass used in calculation are detailed elsewhere [33]. The loading rates in nanoindentation tests were converted into an approximate shear strain rate $\dot{\gamma}_{\mathrm{eff}}$. This was accomplished by first examining the indentation strain rate $\dot{\varepsilon}_i = (1/h)(\mathrm{d}h/\mathrm{d}t)$ and then related to the shear strain rate $\dot{\gamma}_{\mathrm{eff}}$ by $\dot{\gamma}_{\mathrm{eff}} \approx 0.16\dot{\varepsilon}_i$ [14].

Figure 10c shows the plots of numerical values of hardness as a function of shear strain rate calculated for temperatures in the range of 300–400 K. The sensitivity of hardness described by the free volume accumulation–annihilation mechanisms to shear strain rate and temperature is clearly seen. The measured hardness deduced from incremental cyclic loadings are actually an average value resulted from a mixture of propagating shear bands, arrested shear bands and virgin regions. In Fig. 10c, the comparison between numerical and experimental values of hardness illustrates the importance of the dynamic of shear bands propagation where free volume accumulation–annihilation plays a key role on plasticity and the changes of hardness. However, arrested shear bands will not contribute to harden further the metallic glass; this is observed from the quasi-static cyclic loadings. Indeed, the unloading–reloading process in quasi-static cyclic mode at constant $F_{\max} = 3750$ and 2500 μN (data not shown here), all previous shear bands already arrested cause only a weak increase of hardness and the reloading curve deviates from the previous unloading to form an open jaw which corresponds to a softening behaviour. The microscopic model used in this study captures qualitatively well the variation of hardness versus shear strain rate; however, this consistency with available experimental data is still a matter of debate and in need of improvement to include the dynamic of shear bands propagation on local structural changes.

Conclusions

Nanoindentation tests were performed at monotonic, quasi-static and incremental cyclic loadings at various loading rates in the range of 250–2500 μN/s to characterize the effect of cyclic solicitation modes on inelastic deformation behaviour of $Zr_{50}Cu_{40}Al_{10}$ metallic glass. Despite the shape change of inelastic nanoindentation curve from low to high loading rates, atomic force microscopic analyses of remnant indentation morphology reveals an important variation of indents surface in the order of 28% under cyclic loading at constant $F_{\mathrm{Max}} = 3750$ μN. The measured hardness is found to decrease from 6.01 ± 0.15 to 1.74 ± 0.4 GPa after ten cycles at 250 μN/s which is not associated to ISE. However, for a loading rate of 2500 μN/s, the reduction of hardness is in the order of 2.2%. The enhanced inelastic deformation observed is dependent on both loading rate and number of cycles. A slight increase below 5% of contact hardness was identified from incremental cyclic solicitations. Furthermore, a qualitative consistency of the numerical values of hardness versus shear strain rate is found when compared to available experimental data.

Acknowledgements This work was supported by the CMCU_ Hubert Curien program, Award no. 08G1122. The authors would like to thank Professor Y. Yokoyama (Himeji Institute of Technology, Shosha Japan) for providing the sample used in this study.

References

1. Argon AS (1979) Acta Metall 27:47
2. Steif PS, Spaepen F, Hutchinson JW (1982) Acta Metall 30:447
3. Sharma SK, Strunskus T, Ladebusch H et al (2008) J Mater Sci 43(16):5495. doi:10.1007/s10853-008-2834-4
4. Wang WH, Dong C, Shek CH (2004) Mater Sci Eng R 44:45
5. Liu CT, Heatherly L, Easton DS, Carmichael CA et al (1998) Metall Mater Trans A 29(7):1811
6. Johnson WL (1999) MRS Bull 24(10):42
7. El-Deiry A, Vinci P, Barbosa N III, Hufnagel C (2001) MRS Symp Proc 644:L10.2.1
8. Xu Y, Wang YL, Liu XJ et al (2009) J Mater Sci 44(14):3861. doi:10.1007/s10853-009-3523-7
9. El-Hadek MA, Kassem M (2009) J Mater Sci 44(4):1127. doi:10.1007/s10853-008-3194-9
10. Louzguine DV, Kato H, Inoue A (2004) Appl Phys Lett 84:1088
11. Inoue A (2000) Acta Mater 48:279
12. Packard CE, Witmer LM, Schuh CA (2008) Appl Phys Lett 92:171911
13. Yang B, Riester L, Nieh TG (2006) Scripta Mater 54:1277
14. Schuh CA, Lund AC, Nieh TG (2004) Acta Mater 52:5879
15. Yang B, Nieh TG (2007) Acta Mater 55:295
16. Saraswati T, Sritharan T, Mhaisalkar S, Breach CD, Wulff F (2006) Mater Sci Eng A 423:14
17. Zhang Y, Wang WH, Greer AL (2006) Nat Mater 5:857
18. Oliver WC, Pharr GM (1992) J Mater Res 7(6):1564
19. Schuh CA, Nieh TG (2003) Acta Mater 51:87
20. Jiang WH, Atzmon M (2003) J Mater Res 18:755
21. Hajlaoui K, Benameur T, Vaughan G, Yavari AR (2004) Scripta Mater 51:9
22. Bouzakher B, Benameur T, Yavari AR, Sidhom H (2007) J Alloys Compd 434–435:52
23. Khan MK, Hainsworth SV et al (2009) J Mater Sci 44(4):1006. doi:10.1007/s10853-008-3222-9
24. Mukhopadhyay NK, Paufler P (2006) Int Mater Rev 51:209
25. Zhang H, Jing X, Subhash G, Kecskes LJ, Dowding RJ (2005) Acta Mater 53:3849
26. Li N, Liu L, Zhang M (2009) J Mater Sci 44(12):3072. doi:10.1007/s10853-009-3407-x
27. Zhang ZF, Eckert J, Schultz L (2003) Acta Mater 51:1167
28. Mukai T, Nieh TG, Kawamura Y, Inoue A, Higashi K (2002) Scripta Mater 46:43
29. Xu Z-Hi, Li X (2005) Acta Mater 53:1913
30. Schuh CA, Nieh TG (2004) J Mater Res 19:46
31. Spaepen F (1977) Acta Metall 25:407
32. Benameur T, Hajlaoui K, Yavari AR, Inoue A, Rezgui B (2002) Mater Trans JIM 20:2617
33. Yokoyama Y, Fukaura K, Inoue A (2002) Intermetallics 10:1113